Radial-histogram transform of scanning-probe-microscope images

D. Schleef and D. M. Schaefer
Department of Physics, Purdue University, West Lafayette, Indiana 47907

R. P. Andres
School of Chemical Engineering, Purdue University, West Lafayette, Indiana 47907

R. Reifenberger
Department of Physics, Purdue University, West Lafayette, Indiana 47907

(Received 5 October 1995)

A transform is described for analyzing scanning-probe-microscope images. This radial-histogram transform is shown to contain useful information for ascertaining the structure of an object in a scanning-probe-microscope image. The radial-histogram transform also allows quantitative assessment of tip dilation effects. The utility of the transform is illustrated by analyzing a noncontact atomic force microscope image of a nanometer size Au cluster supported on a mica substrate. Using the radial-histogram transform, detailed information about the faceting, structure, and orientation of the supported nanometer-size cluster is obtained. [S0163-1829(96)02819-7]

I. INTRODUCTION

A transform, hereafter referred to as the radial-histogram transform of a scanning-probe image, is described. This transform is useful for identifying the shape and orientation of a three-dimensional object from its scanning-probe image. The histogram is designed to provide statistical information about preferred orientations of surface normal vectors in a scanning-probe image, information that is difficult to ascertain from the image itself. In addition, it is shown that the radial-histogram transform offers advantages in assessing the influence of tip convolution (strictly speaking, dilation) effects.[1,2]

The utility of this transform is demonstrated by analyzing the shape and orientation of a $\sim$20 nm diameter Au cluster supported by a mica substrate from its noncontact scanning probe image. Use of the noncontact scanning-probe technique is appealing, since the interaction between the probe tip and object under study is minimal, resulting in interaction forces less than 0.1 nN. Under these conditions, nanometer-size objects are not swept away or destroyed by the tip during the image acquisition process. In the case of nanometer-size objects, structural details are often masked in the imaging process, due to tip dilation effects. As will be shown below, the radial-histogram transform allows these issues to be addressed in a quantitative way. In what follows, we show that the radial-histogram transform provides clear evidence of surface faceting of metal clusters and also provides information about the tip geometry of the atomic force microscope (AFM) probe. Based on this analysis, we find good evidence that the Au cluster has a truncated octahedral shape.

II. THE RADIAL HISTOGRAM

The radial histogram was developed to provide reliable statistical information about the three-dimensional (3D) shape and orientation of an object from a scanning-probe-microscope image of that object. The radial-histogram transform analyzes the probability distribution of the surface normal vectors of the scanning-probe image of interest. An advantage of the transform is that it provides statistical information about the orientation and shape of an object imaged with finite resolution by a scanning-probe microscope. A by-product of the transform is that when imaging objects, the tip geometry can be quantitatively assessed.

A. General description

A scanning-probe image is comprised of an array of numbers z_{ij}, which represent the height of an object at specified points along an equally spaced grid of points (x_i, y_j) in the x-y plane. This array of numbers can be described as a continuous function $z(x,y)$ that is sampled at discrete intervals. In a traditional analysis of scanning-probe-microscopy data, the z_{ij} are analyzed to provide a topographical image of the object under study. Often, a Fourier transform is used to reveal the underlying periodicity in the image. In what follows, we describe a scheme, which focuses on the direction of the surface normal vector associated with each data point in the z_{ij} array. We show the advantages of studying the statistical distribution of the direction of these vectors for determining structural information about the object under study.

Since the data sampled at discrete intervals do not inherently contain partial derivative data, this information has to be estimated. The method used to estimate partial derivatives was chosen for its computational efficiency. The partial derivatives at a specific interior vertex point P_{ij} [see Fig. 1(a)] is defined as the average of the partial derivatives of the four lines connecting that vertex to neighboring vertices. The derivative is approximated by

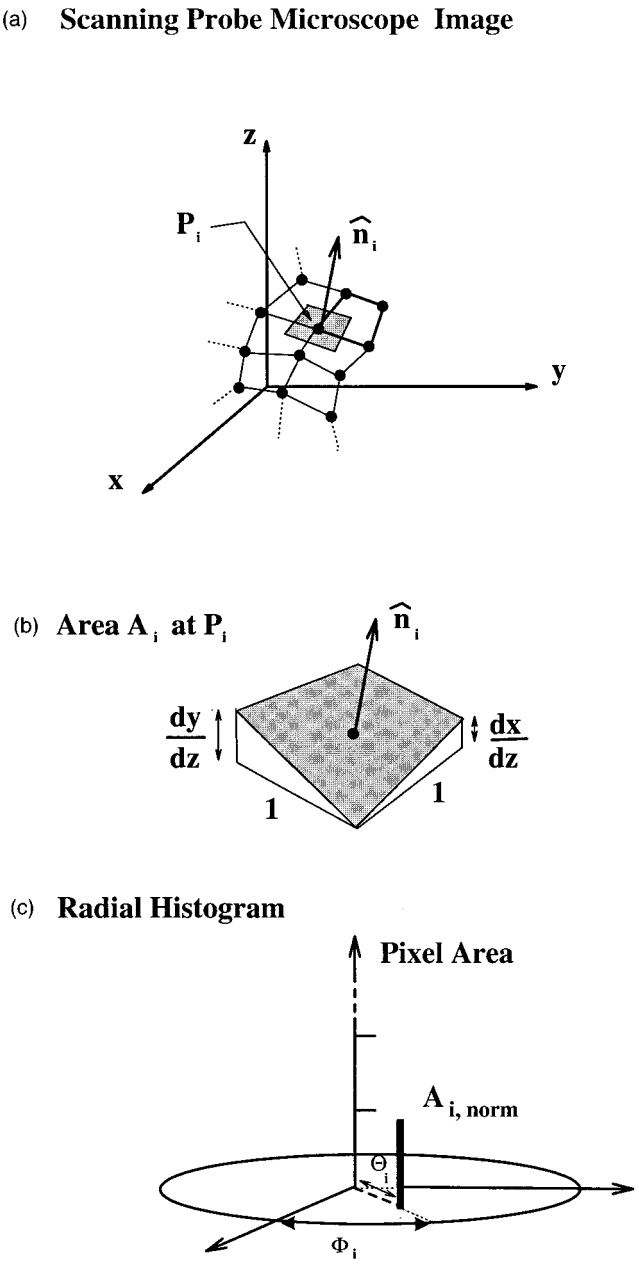

FIG. 1. The definition of a radial histogram. In (a), data points adjacent to the point P_{ij} are used to define a vector normal to the image at point (i,j). In (b), the vector $\vec{n}_{ij}$ can be used to specify the area of a pixel located at P_{ij}. In (c), the area A_{ij} is plotted in circular cylindrical coordinates. The angle ϕ_{ij} defines the azimuthal coordinate, while the perpendicular distance from the z axis is defined by θ_{ij}. This is the first step in the construction of a radial histogram. By studying the distribution of the areas A_{ij} plotted in this way, useful structural information about the scanning-probe image can be obtained.

$$\left.\frac{\partial z}{\partial x}\right|_{ij}=\frac{1}{2}[z_{i+1,j}-z_{i-1,j}], \tag{1}$$

$$\left.\frac{\partial z}{\partial y}\right|_{ij}=\frac{1}{2}[z_{i,j+1}-z_{i,j-1}]. \tag{2}$$

Note that this definition assumes the scanning-probe-microscope data file is equiaxied, i.e., the magnification usually present in the z direction has been properly accounted for. In what follows, we normalize the z-height data by the distance between the data points in the x and y directions (assumed to be equal).

As shown in Fig. 1(b), the vector normal to the area at the point P_{ij} is given by

$$\vec{n}_{ij}=(n_{ij,x},n_{ij,y},n_{ij,z}) \tag{3}$$

$$=\left(-\left[\left.\frac{\partial z}{\partial x}\right|_{ij}\right],-\left[\left.\frac{\partial z}{\partial y}\right|_{ij}\right],1\right). \tag{4}$$

Likewise, the area A_{ij} at P_{ij} is given by

$$A_{ij}=|\vec{n}_{ij}|=\sqrt{1+\left[\left.\frac{\partial z}{\partial x}\right|_{ij}\right]^2+\left[\left.\frac{\partial z}{\partial y}\right|_{ij}\right]^2}. \tag{5}$$

The vector $\vec{n}_{ij}$ can be expressed in terms of spherical components by

$$n_{ij,x}=A_{ij}\sin\theta_{ij}\cos\phi_{ij}, \tag{6}$$

$$n_{ij,y}=A_{ij}\sin\theta_{ij}\sin\phi_{ij}, \tag{7}$$

$$n_{ij,z}=A_{ij}\cos\theta_{ij}=1, \tag{8}$$

where the azimuthal angle

$$\phi_{ij}=\arctan\left[\frac{n_{ij,y}}{n_{ij,x}}\right] \tag{9}$$

(with the quadrant of ϕ_{ij} chosen appropriately) and the polar angle

$$\theta_{ij}=\arccos\left[\frac{n_{ij,z}}{A_{ij}}\right]=\arctan[\sqrt{n_{ij,x}^2+n_{ij,y}^2}] \tag{10}$$

contain the information about the orientation of vector $\vec{n}_{ij}$ normal to the area A_{ij}.

The *distribution* of the directions of the vectors $\vec{n}_{ij}$ perpendicular to the areas A_{ij} contains information that is useful. The angles ϕ_{ij} and θ_{ij} defined above can be used to locate the area A_{ij} in a two-dimensional set of bins defined by a circular cylindrical coordinate system, with the azimuthal angle defined by ϕ_{ij}, and the perpendicular distance from the z axis defined by θ_{ij} [see Fig. 1(c)].

Unlike a regular histogram, multiple bins H_{kl} are filled by the area A_{ij}, in proportion to

$$H_{kl}=\sum_{ij} A_{ij}e^{-\gamma_{kl}^2/\alpha^2}, \tag{11}$$

where γ_{kl} is the angular separation between the bin specified by (θ_k,ϕ_l) and the normal $\vec{n}_{ij}$. To aid in plotting the final histogram, a parameter $\alpha\sim5°$ is included as a smoothing factor.

This procedure is followed, since the bins do not all correspond to the same normal area, i.e., if this scaling is not done, the radial histogram of a sphere will not have a histogram that visually represents equal areas in all directions.

The smoothing factor is used to reduce the noise due to the discrete sampling of $z(x,y)$. In summary, a radial-histogram transform is a way of representing all areas A_{ij} plotted vertically at the position specified by the ϕ_{ij} and θ_{ij} for all data points (i,j) comprising a scanning-probe-microscope image.

An application of the radial histogram discussed below involves an analysis of scanning-probe-microscope images of faceted objects. Because of noise and tip dilation effects, the image of a faceted object may not readily appear to be faceted. A radial histogram of this image, however, will have peaks that represent these facets. It should be noted, however, that two facets on an object having the same normal will only produce one peak in the radial histogram. In this way, it is possible for different images to produce the same radial histogram. However, by selecting subsets of an image, one can usually assign peaks in the histogram to their corresponding facets.

A number of procedures have been developed that enhance the appearance of the histogram. To prevent structural information about the (nominally) flat substrate from cluttering the histogram at $\theta=0$, a small hole is cut in the histogram and data at angles θ less than 10° are not plotted. When this information is included, there will be a large peak in the center, corresponding to the flat substrate. The width of this peak is related to the smoothness of the substrate. Work with the histogram has shown that the information contained can be enhanced in one of two ways. In a standard histogram plot, the radial angle ϕ is distinguished using a color wheel scheme to allow for better viewing. The histogram can also be represented using a contour format that is better suited for peak identification and quantitative analysis of the information.

B. A simple example; the radial histogram of a cube

To better illustrate the utility of the radial-histogram transform, a simple example is discussed. The shape and orientation of a cube is analyzed using the normal radial-histogram method. This test object was chosen to provide an intuitively simple way to illustrate the utility of the radial-histogram transform. Furthermore, this simple example shows how the effect of tip dilation can also be addressed.

Figure 2(a) shows a computer generated scanning-probe image of a cube along with its radial histogram [see Fig. 2(b)]. In this example, no tip dilation is included. The radial histogram has been assigned colors, for ease in identification of the various features that appear. The color red has been chosen to coincide with $\phi=0$. This color mapping can be transferred back to the original object and is useful for highlighting any faceting that may be contained in the scanning-probe image. The radial histogram for a cube shows four peaks of equal height located at the azimuthal angles of 0, $\pi/2$, π, and $3\pi/2$. The presence of these peaks represents the probability that unit vectors pointing in these four directions are present in the object under consideration. The equal height of each peak reflects the fact that the facets of the object under study have equal areas. The central peak at $\theta=0$, originating from the top of the cube, is suppressed, because it coincides with the peak from the flat substrate on which the cube rests. Any small features located in the interior region of the radial histogram are computational artifacts

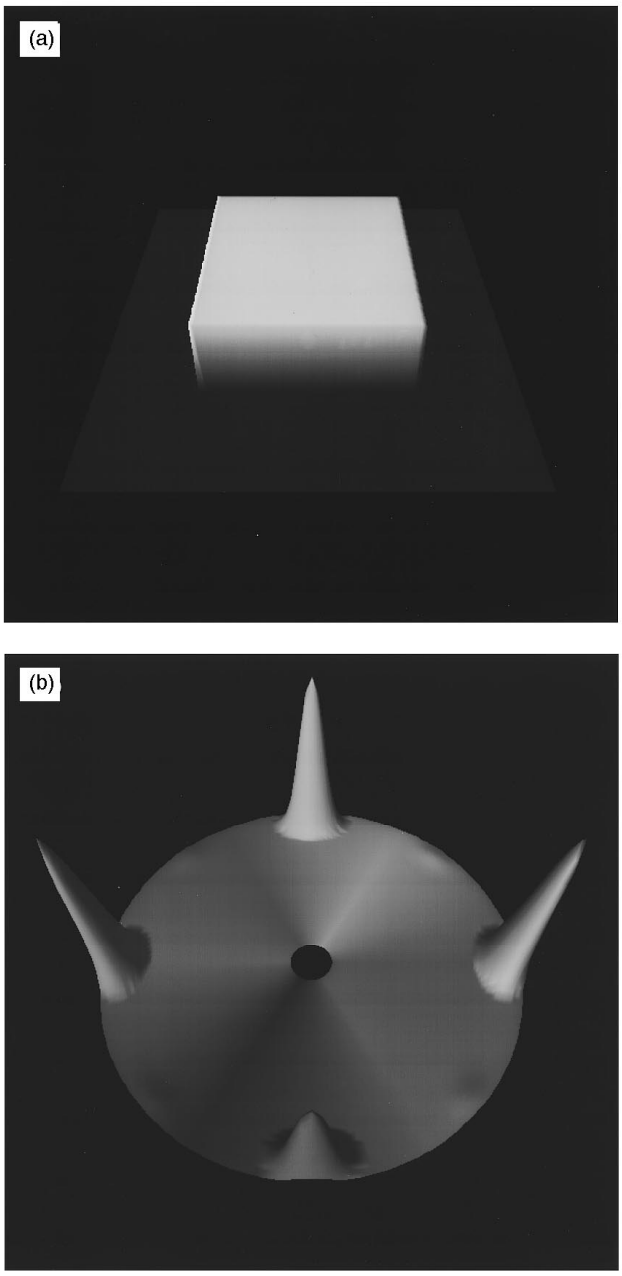

FIG. 2. (a) A computer generated cube and (b) its radial-histogram transform.

introduced by the numerical generation of the cube on the computer. In essence, all sharp edges are lost, due to the finite resolution of the generated image. These effects could be minimized using a more densely packed grid, but it is useful to maintain the same number of grid points found in experimental scanning-probe data.

The influence of tip dilation on the radial histogram of a cube is illustrated Fig. 3(a). In this figure, the image of the cube was generated using a conical tip of half angle 30°. The radial histogram of this dilated image contains a number of important features. First, the four peaks in 2(b) have been shifted inward and are now centered at an angle of $\theta_p=60°$. This is a direct consequence of the dilation process and can be used to determine α, the half angle of the tip by the formula

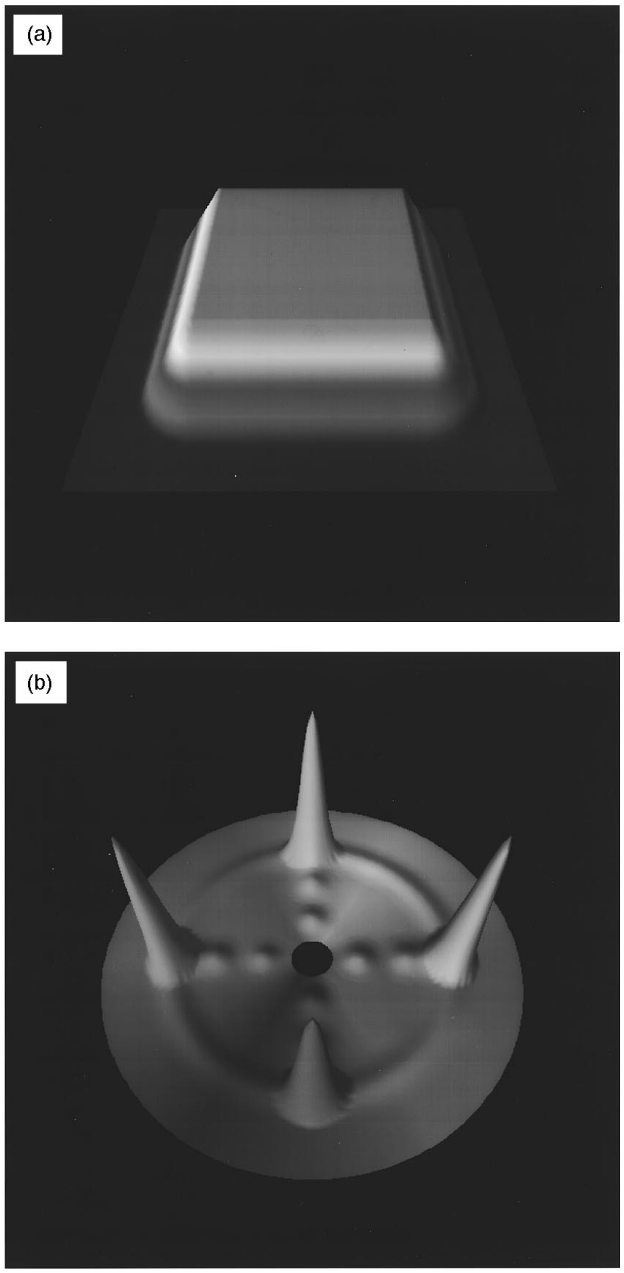

FIG. 3. The effect of tip dilation on a cube. In (a), the calculated scanning-probe image of a cube dilated with a conical tip of half angle $\alpha = 30°$ and (b) the resulting radial-histogram transform. The location of the peaks in the transform and the symmetrical shape of the dilation skirt provide information about the tip shape used to produce the image.

$$\alpha = \pi/2 - \theta_p . \tag{12}$$

Second, the peaks are now connected by a ringlike skirt that contains important information about the tip shape. The ringlike feature also appears at $\theta = 60°$ for all ϕ, indicating that a symmetrical tip was used when calculating the image in Fig. 3(a). As will be seen below, asymmetry in the dilation skirt in actual data provides valuable information about the overall tip shape.

This example illustrates the advantages of a radial-histogram transform in determining the structure of an object and the effects of tip dilation in a scanning-probe image. In what follows, we apply this transform to determine the structure and orientation of a supported nanometer-size cluster of Au.

III. AN EXAMPLE: STRUCTURE AND ORIENTATION OF A SUPPORTED NANOMETER-SIZE CLUSTER

A. Overview

The structure and stability of nanometer-size clusters has been a topic of considerable interest. Traditionally, the structure of a small metallic cluster has only been accessible using high resolution transmission electron microscopy (HRTEM) techniques.[3] Interestingly, HRTEM lattice images of nanometer-size metallic particles have provided evidence for structural fluctuations in the shape and orientation of a supported cluster.[4] The origin of these structural fluctuations, especially if they represent an inherent structural instability at the nanometer length scale, is of considerable interest and many studies attempting to provide further insight into this important issue have recently appeared.[5–14]

It has recently been reported that noncontact scanning-probe microscopy provides a way to image clusters deposited on atomically flat substrates.[15,16] Evidently, when using the AFM in the noncontact mode, the problem of tip-induced cluster motion observed in the early cluster studies[17] are eliminated. In what follows, the structure and orientation of a $\sim$20 nm diameter Au cluster is analyzed by applying the radial histogram transform to its scanning-probe image. The analysis provides clear evidence that the structure and orientation of supported nanometer-size clusters are accessible using the scanning-probe technique.

B. Cluster source

Before analyzing the scanning-probe image, it is useful to briefly review how the Au clusters are produced. The clusters used in this study were prepared using a multiple expansion cluster source (MECS), as described elsewhere.[18,19] Briefly, it is a gas aggregation source, that is designed to run with 20–50 Torr of inert gas in the growth region. Both cluster growth via accretion of single atoms and via cluster-cluster aggregation can be promoted. In the present experiment, Au clusters with diameters as large as 20 nm were produced by aggregation of primary clusters with diameters in the 1–1.5 nm range. As in previous studies,[20–24] cluster samples were captured either on substrates for scanning-probe analysis or on suitable amorphous carbon grids for further analysis by TEM. Previous TEM studies of clusters studied in this way have confirmed the ability of the MECS to produce metal clusters having a controlled mean size and a narrow size distribution.[18]

The experimental image discussed below was obtained from an *annealed* cluster deposited onto a mica substrate. To produce an annealed cluster, a dilute stream of Au clusters surrounded in an He carrier gas was directed through a tubular annealing reactor consisting of an alumina tube passing through a Lindberg furnace. The mean residence time of a cluster in the tube is approximately one second. With this arrangement, clusters passing from the growth region of the MECS at 300 K could be heated to a predetermined temperature and then cooled again to 300 K before deposition. After

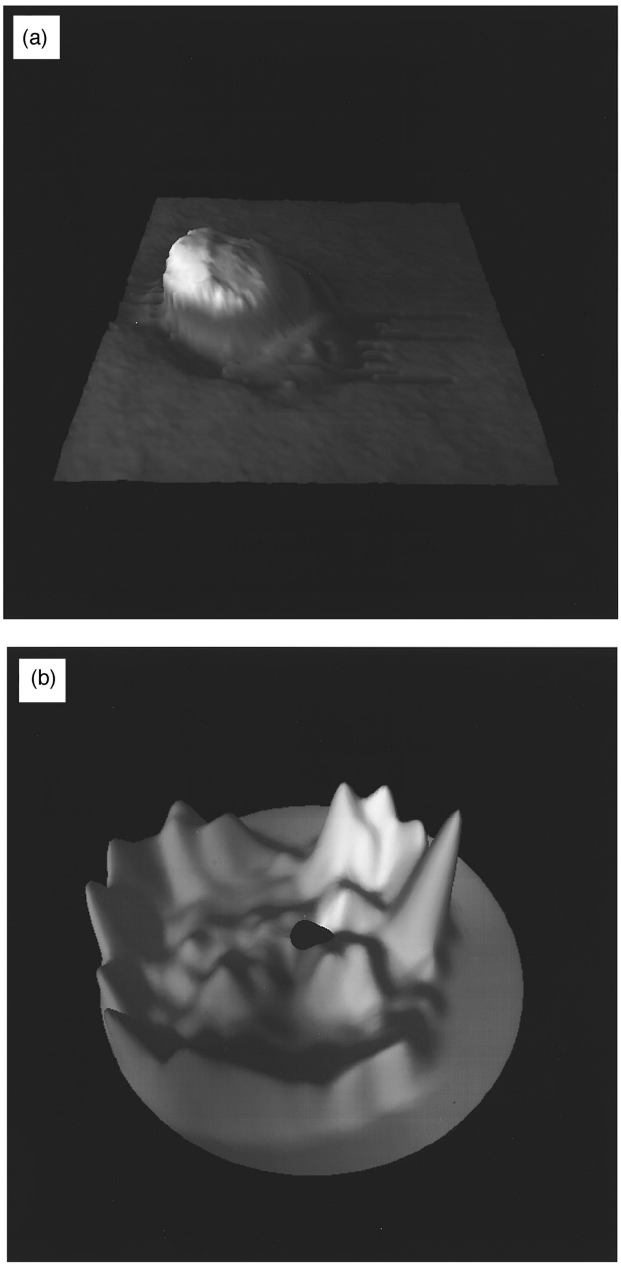

FIG. 4. (a) Experimental image obtained from a noncontact atomic force microscope of a Au cluster and (b) a radial-histogram transform of the image. In (c), a contour plot of the transform is also given. The three interior peaks in this contour plot correspond to facets in the original image and are labeled *A*, *B*, and *C* for identification purposes.

annealing, the clusters pass into a vacuum chamber with a base pressure of 1×10^{-6} Torr and are deposited onto carbon coated TEM grids (carbon film thickness 5 nm) or a suitable substrate (in this case mica) for future scanning-probe studies.

C. AFM characteristics

The AFM used was a custom-built instrument operating in either an ambient or vacuum environment and capable of scanning in either the contact or noncontact mode. Cluster-covered substrates are mounted onto a segmented, 1.27 cm long PZT-5A piezoelectric tube. A second piezoelectric tube is used to hold a commercially available AFM Si ultralever.[25] This second piezo tube allows for the oscillatory motion of the tip during noncontact operation and cantilever calibration. Detection of the cantilever displacement utilizes the laser deflection method,[26,27] in which a focused laser beam is reflected off the back of the cantilever onto a split photodiode position sensing detector (PSD). The output of the PSD is read by a 68030 CPU based computer system. The computer handles all data acquisition and system control.

All noncontact mode scans were performed using an amplitude modulation technique. When the separation distance between the cantilever tip and substrate becomes $\leqslant 10$ nm, attractive forces produce a shift in the cantilever resonant frequency, producing a change in the amplitude of oscillation, as measured by a lock-in amplifier. Digital feedback utilizing the lock-in output was used to keep the resonant frequency constant, corresponding to a constant separation between tip and substrate. When operating in the noncontact mode, the height resolution was estimated to be $\sim$ 0.2–0.5 nm.

An important feature of the instrument used in this study is that the AFM apparatus was enclosed in a small stainless

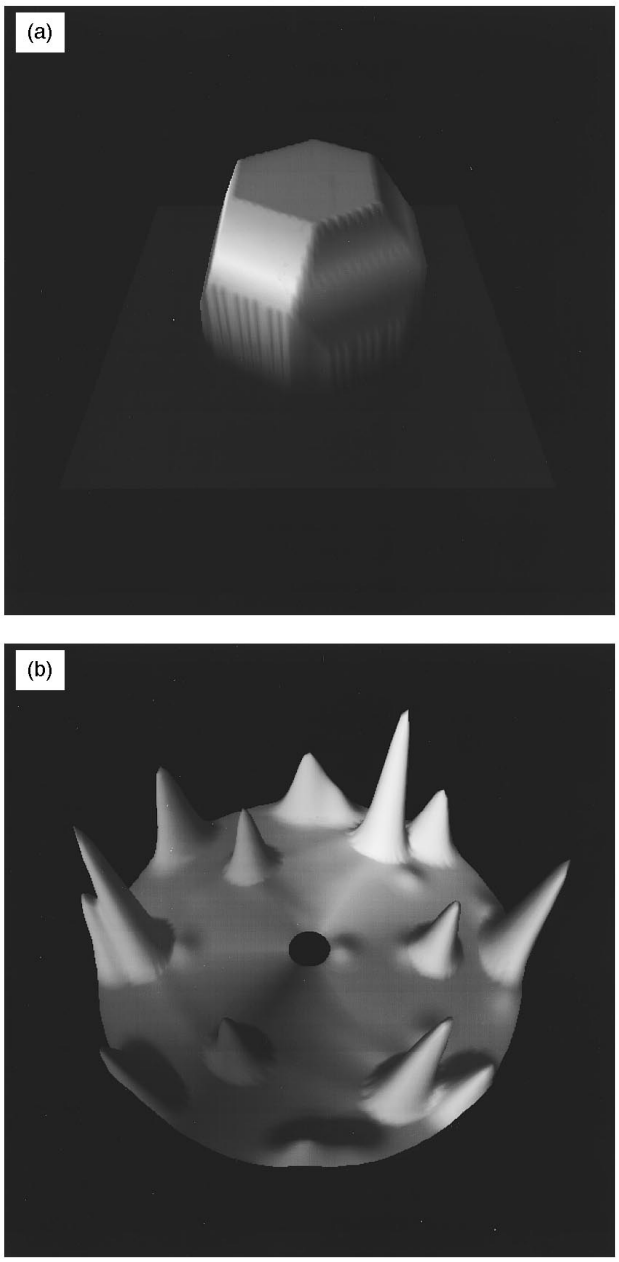

FIG. 5. (a) A model of a truncated octahedron with a hexagonal facet parallel to the substrate and (b) its radial-histogram transform.

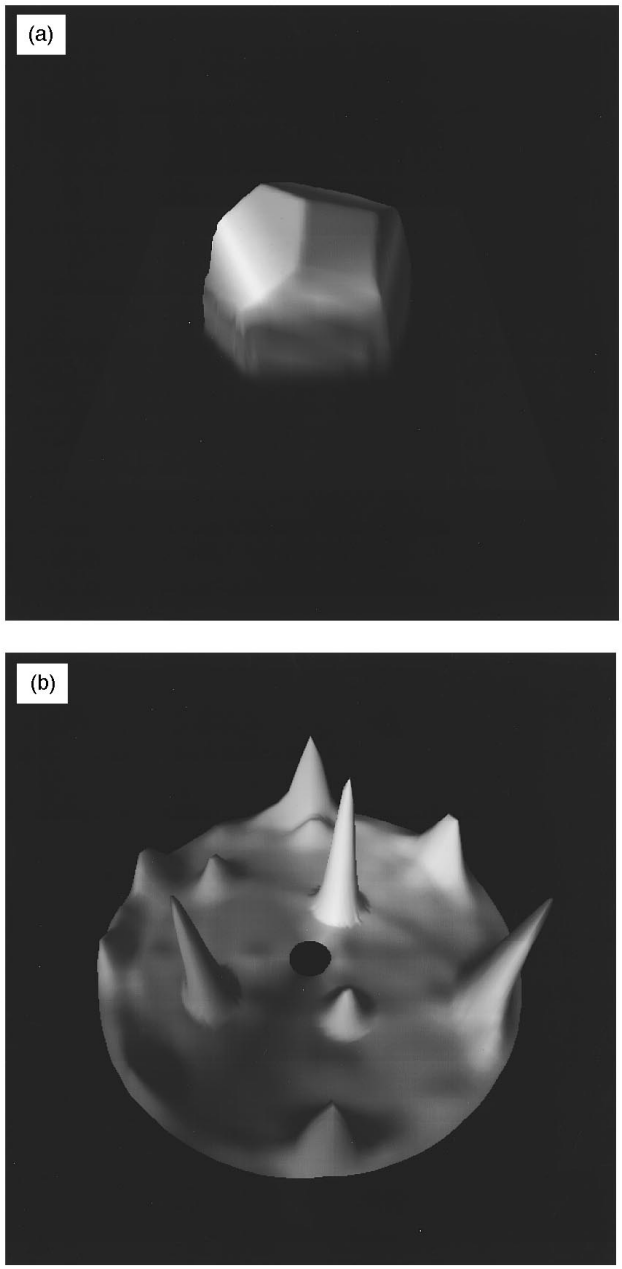

FIG. 6. An illustration of (a) a truncated octahedron tilted through an angle of 32° and (b) the resulting radial histogram.

steel chamber that was pumped to a pressure of ~500 mTorr. Under these conditions, layers of adsorbed water or other volatile substances do not coat the substrate or tip, thus allowing improved operation of the instrument.

D. Cluster structure

Before proceeding, some background information on the expected cluster structure is required. Previous studies of the annealed MECS clusters have been reported in which HRTEM studies were performed on deposited clusters as a function of the temperature of the annealing reactor.[14] The results of these experiments can be summarized as follows.

(i) Without annealing, the clusters are multiply twined polycrystals with fcc domains between 1 and 2 nm in diameter.

(ii) When the clusters are annealed at 1200 K (a temperature sufficient to melt Au clusters with diameters less than ~7.5 nm), all clusters with diameters greater than ~ 8 nm were found to have a multiply twined polycrystalline motif. Several symmetrical multiply twined polycrystal's (both icosahedra and decahedra) were observed. All clusters with diameters less than ~8 nm and showing clear (111) lattice fringes were unambiguously identified as single fcc crystals.

(iii) When the clusters are annealed at 1400 K (above the bulk melting temperature of Au), all clusters oriented in such a way as to show clear (111) lattice fringes, could be unambiguously identified as single fcc crystals.

E. Radial histogram transform of a supported Au cluster

Figure 4(a) shows a representative noncontact mode AFM image of a supported Au cluster. The image is 60 nm by 60

TABLE I. Comparison of the position of interior peaks measured from an experimental scanning-probe image and a model truncated octahedron tilted through an angle of 32°.

Peak ID	Experiment		Calculated	
	θ	ϕ	θ	ϕ
A	22°	50°	31°	65°
B	39°	211°	44°	203°
C	17°	292°	31°	295°

nm in extent. The total z-height variation is 20 nm. Careful examination of the image shows distinct hints of a faceted object, but it is difficult to extract quantitative information about the structure and orientation of the object producing the image. Furthermore, tip dilation effects cause the usual smearing of any sharp features that might help in this analysis. The radial-histogram transform, however, is an ideal way to analyze this image.

The radial-histogram transform of this image is shown in Fig. 4(b). In this case, a window was superimposed on the image to select out only the region of interest. However, unless the window is very tightly positioned over the object under analysis, regions of the substrate are inevitably included in the analysis, hence the need to suppress plotting of data for $\theta<10°$. A contour plot of the radial-histogram transform is shown in Fig. 4(c).

The presence of sharp peaks in the radial histogram clearly indicates the presence of a faceted structure. Furthermore, other images from the same cluster showed similar structure when analyzed by the radial histogram. As discussed below, analysis of the angular separation between the interior peaks permits a quantitative interpretation of the AFM image.

The cluster studied was prepared using the procedure described in Sec. III B. Energy minimization calculations indicate that the lowest potential energy shape for a cluster of Au atoms is a truncated octahedron.[28] In what follows, we therefore test to see how consistent the radial-histogram transform is with a model structure having this geometry.

Figure 5(a) shows a computer-generated truncated octahedron resting on with a hexagonal facet against the supporting plane. The resulting radial-histogram transform is shown in Fig. 5(b). The six interior peaks in the computer-generated histogram correspond to six of the facets of the truncated octahedron. The two different heights of the peaks reflect the different areas of the square and hexagonal facets of a truncated octahedron. The 12 features located near $\theta=90°$ correspond to vertical faces produced by the reentrant nature of the object. The position of these peaks in experimental data is influenced by tip dilation effects. Noncontact AFM imaging is not capable of resolving the reentrant facets, but as shown in Fig. 5(b), information about the edges bounding these reentrant facets are accessible.

There are noticeable differences when Fig. 4(b) is compared to Fig. 5(b). First, the peaks in the histogram generated from the data are wider than the peaks generated by the model, since the noise in the data spreads the peaks and the faceting on the cluster is not as well defined as in the model. Second, the position of the peaks in the computer-generated histogram do not match with those observed experimentally, suggesting the possibility of a tilt of the cluster on the substrate.

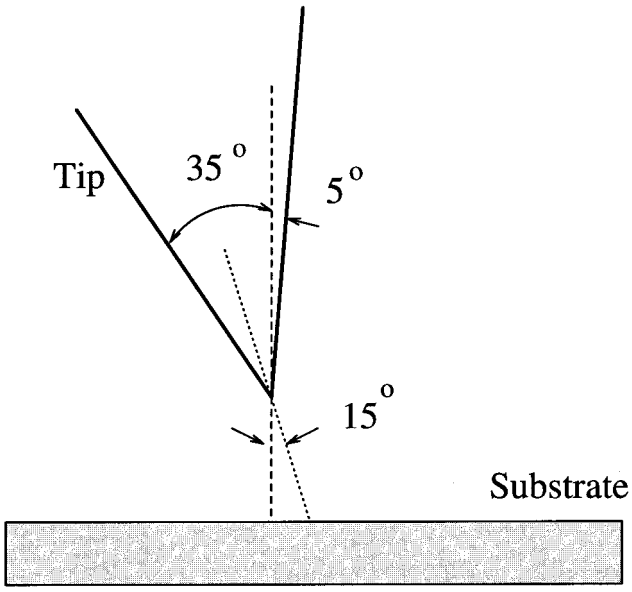

FIG. 7. The overall tip shape determined from the radial histogram. A symmetric tip of half angle ~20° can be inferred by allowing for a ~15° tilt angle between tip and substrate as indicated.

In an effort to better compare the radial histogram of the cluster image to the transform of the truncated octahedral model, a sequence of radial-histogram transforms were calculated, including an adjustable tilt of a truncated octahedron with respect to the substrate. The calculation was repeated until a tilt angle was found that minimized the difference between peak positions in the calculated and experimental radial-histogram transforms.

The best fit to the experimental data is shown in Fig. 6. The position of the exterior peaks depend on the shape of the tip in a complicated way, and will not be analyzed any further. The angles between the three interior peaks are useful for identifying the structure of the supported cluster. The angular positions of the three interior peaks obtained from Fig. 4(c) are compared to the known values for a truncated octahedron (see Table I). The angular separation of the interior peaks are reproduced to within ~15°, a result which supports the truncated octahedral model. The calculated transform did not reproduce the relative heights of the peaks shown in Fig. 4(b), suggesting that the relative areas of the faceted cluster are not accurately described by the perfect octahedral model considered here.

The reason for choosing a truncated octohedron is related to considerations outlined in Sec. III D. Other possible crystalline objects might also be considered. Although there are many such objects, the choice is limited by the number of peaks that fall within the dilation skirt. Most other crystalline objects will produce more than three facets inside the dilation skirt. In addition, the number of peaks on the edge of the skirt has significance and will differ between crystalline objects. Based on these considerations, the truncated octahedron model seems to provide the best fit to the experimental image at this time.

An important feature evident from Fig. 4(b) is the presence of an asymmetric boundary in the histogram. This boundary is attributed to tip dilation effects. Analysis of the dilation skirt provides information about the tip shape. For instance, for $\phi=\pi$, the skirt is bounded by $\theta\simeq 55°$, while for $\phi=3\pi/2$, the skirt is bounded by $\theta\simeq 85°$. These angles correspond to a linear scan in the x direction. This information requires an asymmetric tip half angle of $\alpha\simeq 5°$ and $\alpha\simeq 35°$, respectively. A symmetric tip of half angle 20° with overall tilt angle between the tip and substrate of $\sim 15°$ would produce this effect (see Fig. 7).

IV. SUMMARY AND CONCLUSIONS

A radial-histogram transform has been defined and shown to contain valuable information about the orientation and structure of an object imaged by a scanning probe microscope. Furthermore, by studying the symmetry and location of the dilation skirt of the histogram, useful information about the symmetry and shape of the scanning probe tip can be quickly obtained and used to characterize the quality of the tip under study.

To illustrate the utility of the radial-histogram transform, an analysis of a noncontact mode image of a supported nanometer-size Au cluster was performed. The particular cluster studied was annealed to produce a crystalline cluster and deposited on a mica substrate. The noncontact AFM image showed hints of distinct facets, but little quantitative information about the overall structure. In contrast, analysis of the radial-histogram transform of this image provided clear evidence for faceting and a model for the shape and orientation of the cluster on the substrate.

It seems likely that this radial-histogram transform will find wide-spread use. It provides a generalized, quantitative method of determining not only the surface structure and orientation of nanometer-scale objects, but also provides information about the tip geometry of the AFM probe.

Note added in proof. A color copy of the figures in this manuscript is available upon request from R. Reifenberger (electronic address: rr@physics.purdue.edu).

ACKNOWLEDGMENT

This work was partially funded by the National Science Foundation under Contract No. 9522248-CTS.

[1] J.S. Villarrubia, Surf. Sci. **321**, 287 (1994).
[2] J.S. Villarrubia, J. Vac. Sci. Technol. B **14**, 1518 (1996).
[3] L.D. Marks, Rep. Prog. Phys. **57**, 603 (1994).
[4] S. Iijima and T. Ichihashi, Phys. Rev. Lett. **56**, 616 (1986).
[5] M.R. Hoare and P. Pl, J. Cryst. Growth **17**, 771 (1972).
[6] P.M. Ajayan and L.D. Marks, Phys. Rev. Lett. **60**, 585 (1988).
[7] P.M. Ajayan and L.D. Marks, Phys. Rev. Lett. **63**, 279 (1989).
[8] S. Iijima and T. Ichihashi, Mat. Trans. J.I.M. **31**, 582 (1990).
[9] P. Williams, Appl. Phys. **50**, 1760 (1987).
[10] A. Howie, Nature **320**, 684 (1986).
[11] T. Kizuka, T. Kachi, and N. Tanaka, Z. Phys. D **26**, S58 (1993).
[12] D. Narayanaswamy and L.D. Marks, Z. Phys. D **26**, S70 (1993).
[13] D. Reinhard, B.D. Hall, D. Ugarte, and R. Monot, Z. Phys. D **26**, S76 (1993).
[14] A.N. Patil, D.Y. Paithankar, N. Otsuka, and R.P. Andres, Z. Phys. D **26**, 135 (1993).
[15] D.M. Schaefer, A. Ramachandra, R.P. Andres, and R. Reifenberger, Z. Phys. D **26**, S249 (1993).
[16] D.M. Schaefer, A. Patil, R.P. Andres, and R. Reifenberger, Appl. Phys. Lett. **63**, 1492 (1993).
[17] A.M. Baro, A. Bartolome, L. Vazquez, N. Garcia, R. Reifenberger, E. Choi, and R.P. Andres, Appl. Phys. Lett. **51**, 1594 (1987).
[18] E. Choi and R.P Andres, in *Physics and Chemistry of Small Clusters*, edited by P. Jena, B.K. Rao, and S.N. Khanna (Plenum, New York, 1987), p. 61.
[19] T. Castro, Y.Z. Li, R. Reifenberger, E. Choi, S.B. Park, and R.P. Andres, J. Vac. Sci. Technol. A **7**, 2845 (1989).
[20] M.E. Lin, R. Reifenberger, and R.P. Andres, Phys. Rev. B **46**, 15 490 (1992).
[21] M.E. Lin, R. Reifenberger, A. Ramachandra, and R.P. Andres, Phys. Rev. B **46**, 15 498 (1992).
[22] T. Castro, R. Reifenberger, E. Choi, and R.P. Andres, Surf. Sci. **234**, 43 (1990).
[23] T. Castro, R. Reifenberger, E. Choi, and R.P. Andres, Phys. Rev. B **42**, 8548 (1990).
[24] T. Castro, E. Choi, Y.Z. Li, R.P. Andres, and R. Reifenberger, in *Clusters and Cluster-Assembled Materials*, edited by R.S. Averback, J. Bernholc, and D.L. Nelson, MRS Symposia Proceedings No. 206 (Materials Research Society, Pittsburgh, 1991), p. 159.
[25] Available from Park Scientific Instruments, Sunnyvale, CA 94089.
[26] G. Meyer and N.M. Amer, Appl. Phys. Lett. **53**, 1045 (1988).
[27] G. Meyer and N.M. Amer, Appl. Phys. Lett. **53**, 2400 (1988).
[28] D.Y. Paithankar, J. Talbot, and R.P. Andres (private communication).